Atmos. Chem. Phys., 15, 10567–10579, 2015
www.atmos-chem-phys.net/15/10567/2015/
doi:10.5194/acp-15-10567-2015

Atmospheric Chemistry and Physics
Open Access

NO_2 seasonal evolution in the north subtropical free troposphere

M. Gil-Ojeda[1], M. Navarro-Comas[1], L. Gómez-Martín[1,2], J. A. Adame[1], A. Saiz-Lopez[3], C. A. Cuevas[3], Y. González[4], O. Puentedura[1], E. Cuevas[4], J.-F. Lamarque[5], D. Kinninson[5], and S. Tilmes[5]

[1]Instituto Nacional de Técnica Aeroespacial, Torrejón de Ardoz, Spain
[2]Groupe de Spectrométrie Moléculaire et Atmosphérique, URM CNRS 7331, UFR Sciences Exactes et Naturelles, Moulin de la Housse, BP 1039, 51687 Reims CEDEX 2, France
[3]Atmospheric Chemistry and Climate Group, Institute of Physical Chemistry Rocasolano, CSIC, Madrid, Spain
[4]Izaña Atmospheric Research Center, AEMET, Tenerife, Spain
[5]Atmospheric Chemistry Division, NCAR, Boulder, CO, USA

Correspondence to: M. Gil-Ojeda (gilm@inta.es)

Received: 20 February 2015 – Published in Atmos. Chem. Phys. Discuss.: 22 May 2015
Revised: 6 September 2015 – Accepted: 7 September 2015 – Published: 25 September 2015

Abstract. Three years of multi-axis differential optical absorption spectroscopy (MAXDOAS) measurements (2011–2013) have been used for estimating the NO_2 mixing ratio along a horizontal line of sight from the high mountain subtropical observatory of Izaña, at 2370 m a.s.l. (NDACC station, 28.3° N, 16.5° W). The method is based on horizontal path calculation from the O_2–O_2 collisional complex at the 477 nm absorption band which is measured simultaneously to the NO_2 column density, and is applicable under low aerosol-loading conditions.

The MAXDOAS technique, applied in horizontal mode in the free troposphere, minimizes the impact of the NO_2 contamination resulting from the arrival of marine boundary layer (MBL) air masses from thermally forced upwelling breeze during middle hours of the day. Comparisons with in situ observations show that during most of the measuring period, the MAXDOAS is insensitive or very slightly sensitive to the upwelling breeze. Exceptions are found for pollution events during southern wind conditions. On these occasions, evidence of fast, efficient and irreversible transport from the surface to the free troposphere is found.

Background NO_2 volume mixing ratio (vmr), representative of the remote free troposphere, is in the range of 20–45 pptv. The observed seasonal evolution shows an annual wave where the peak is in phase with the solar radiation. Model simulations with the chemistry–climate CAM-Chem model are in good agreement with the NO_2 measurements, and are used to further investigate the possible drivers of the NO_2 seasonality observed at Izaña.

1 Introduction

Nitrogen oxides play an important role in tropospheric chemistry as they control O_3 photochemical catalytic production (Crutzen, 1979), the abundance of hydroxyl radicals, and they contribute to the formation of nitrate aerosols. In a background unpolluted atmosphere where NO_x concentrations are low, net ozone loss occurs during photochemically active periods (Liu et al., 1983; Isaksen et al., 2005). NO_x abundance is highly variable since it is influenced by non-steady natural and anthropogenic emissions and its global distribution is still uncertain. Free troposphere (FT) source inventories indicate that major production comes from lightning (2–16 Tg N yr^{-1}), followed by NH_3 oxidation (0.3–3 Tg N yr^{-1}), stratospheric intrusion (0.08–1 Tg N yr^{-1}) and aircraft (0.6-0.7 Tg N yr^{-1}). Contribution from the boundary layer in remote regions is rare (Bradshaw et al., 2000).

Information about surface NO_x in polluted areas is available due to extended governmental air-quality networks. During the last decade, satellite instruments have demonstrated a capability for successful retrieval of tropospheric NO_2, identifying enhanced concentrations over urban and industrial areas in the boundary layer (Richter et al., 2005; Irie et al., 2005) and tracking the temporal trends (Hilboll et al., 2013; Cuevas et al., 2014). However, direct NO_2 measurements in the background FT are scarce due to the requirement of observational platforms above, typically, 2000 m a.s.l., but also due to the low concentrations present at those levels.

Airborne NO_2 measurements have been performed for decades (Ridley et al., 1988; Carroll et al., 1990); however the need for very short response times at concentrations close to the instrumental detection limit make the FT observations a challenging task. Even though well-characterized aircraft instruments reach detection limits as low as 10 pptv (Heland et al., 2002), few studies are reported in the literature. Measurements are generally collected during individual field campaigns associated to specific targets such as chemistry missions or satellite validations (Jacob et al., 2003; Bucsela et al., 2008; Boersma et al., 2008; Baidar et al., 2013; Flynn et al., 2014). These time and space sparse data limit the study of seasonalities or trends in the FT. Only recently, attempts to obtain global FT NO_2 abundances from a satellite OMI instrument has been performed for the first time (Choi et al., 2014) by using the cloud-slicing technique (Ziemke et al., 2001). The method is based on the comparison of cloud and cloudless scenes to derive the FT mean concentrations. Results show that valuable information on NO_2 large-scale phenomena can be derived from areas where cloud presence is frequent, but does not provide results in places such as at east Atlantic subtropical latitudes, where high pressure is a dominant feature.

Instruments operating in the few high mountain stations existent around the world are the only alternative to monitor NO_2 in the background FT. However, the in situ measurements are often affected by the "upslope breeze effect" (Kleissl et al., 2007; Val-Martin et al., 2008; Rodríguez et al., 2009; Reidmiller et al., 2010; Cuevas et al., 2013). Radiative heating in the mountain slopes results in air upwelling from the boundary layer, contaminating the daytime measurements by generally larger values over the polluted lower layers.

Recently, Gomez et al. (2014) presented a simple method based on a modified geometrical approximation (MGA) to estimate concentrations of trace gases at the level of the Izaña observatory from multi-axis differential optical absorption spectroscopy (MAXDOAS) measurements. The horizontal path length is obtained from the oxygen collisional complex (O_4, hereafter) simultaneously measured with the tracer under consideration (NO_2 and O_3). Gomez et al. (2014) examined a short summer period to demonstrate the validity of the method. Here we apply the same technique to data covering 3 full years (2011–2013) to analyze the seasonal evolution of the NO_2 concentrations in volume mixing ratio (vmr). MAXDOAS present two main advantages with respect to the in situ instrument at this location, both related to the very long optical path of the measurements of over 60 km. Firstly, it minimizes the potential contribution of NO_2 that may be upwelled from the marine boundary layer (MBL). The breeze layer has a limited vertical extension and its relative contribution to the MAXDOAS long path is small. On the contrary, Izaña in situ data around noon are strongly influenced by the underlying polluted MBL (Puentedura et al., 2012; Gomez et al., 2014). Secondly, due to the long light paths achieved by MAXDOAS in the FT, very low concentrations, of a few parts per trillion, can be measured.

Section 2 presents the method, its limits and its associated errors. In Sect. 3 the station and data sets are depicted. Section 4 describes the method used for the retrieval of profiles. The description of the chemical and back trajectories models is done in Sect. 5. Finally, Sects. 6 and 7 present the results and discussion, and summary, respectively.

2 Instrument and methodology

In the year 2010, the DOAS (differential optical absorption spectroscopy) spectrometer, operating in zenith mode at that time, was upgraded for MAXDOAS measurements. The spectrometer records the sky spectrum in the visible range at a spectral resolution of 0.55 nm in 10 elevation angles from -1 to 90°, and 1° field of view, covering a full cycle in 20 min. The number of cycles per day ranges from 26 at winter solstice to 38 in summer. NO_2 is evaluated in the 425–520 nm range in order to simultaneously retrieve the O_4 from the 477 nm absorbing band. The scanning plane is at 0° azimuth (north) to minimize the dependence of the path with the azimuth (Wittrock et al., 2004). The instrument is part of the Network for the Detection of the Atmospheric Composition Change (NDACC) and other settings are those recommended for DOAS-type spectrometers. NO_2 at 294 K temperature from Vandaele et al. (1998) and O_4 from Hermans (2011) cross sections have been used. Details of the instrument, settings and operational mode can be found in Puentedura et al. (2012) and Gomez et al. (2014).

The modified geometrical approximation (MGA) described in Gomez et at. (2014) has been used for the data analysis. NO_2 vmr at the level of the station is obtained by dividing the differential slant column density (DSCD) measured in the horizontal geometry by the horizontal optical path. The DSCD is obtained by subtracting the measurement obtained at the zenith (SZA = 90°) from the measurement in the horizontal path. In a first approximation, the slant paths' contributions of 0 and 90° geometries are cancelled out, and only the signal of the tracers present in the horizontal path remains (see Gomez et al., 2014 for details). The method assumes a quasi-Rayleigh atmosphere, i.e., very low aerosol optical depth (AOD), and a single scattering before the photon reaches the detector. The path is obtained from the O_4 horizontal column since the amount of O_2 is known from the independent air pressure measurements. The path length is then corrected to account for the differences in wavelengths between the O_4 and NO_2 analysis ranges. In practice, the scattering of the zenith path does not take place near the instrument but at a few kilometers above the level of the station. The actual concentration of a measured species X at the station level is given by

$$X_{\mathrm{vmr}} = \frac{X_{\mathrm{DSCD}}}{\frac{\mathrm{O_4DSCD}}{[\mathrm{O_4}]_{\mathrm{surface}}} \cdot f + c}, \quad (1)$$

where X_{DSCD} and $O_{4\mathrm{DSCD}}$ are the slant measured columns of the species X and O_4, respectively. $[O_4]_{\mathrm{surface}}$ is the O_4 at the level of the station, f is the correction factor due to differences in wavelength absorption ranges of the species under study, with respect to O_4 that can be computed from a radiative transfer model (RTM), and c is the error of the approach. The latter is a factor accounting for the dependence with the different vertical distributions of both species and air mass factors (AMF):

$$c = h(Rg - R'g'), \tag{2}$$

where h is the effective scattering height of the vertical ray. R and R' are the ratio of the mean concentration of the layer divided by the concentration at the level of the station of tracer X and O_4, respectively, and g and g' account for their AMF in the zenith geometry ($g = \mathrm{AMF(SZA)} - 1$), where SZA stands for solar zenith angle.

The effective scattering height is defined as

$$h(z) = \sum_{\mathrm{surface}}^{\mathrm{top}} \left(\frac{I(z)}{\int_{\mathrm{surface}}^{\mathrm{top}} I(z)\mathrm{d}z} z \right), \tag{3}$$

where $\frac{I(z)}{\int_{\mathrm{surface}}^{\mathrm{top}} I(z)\mathrm{d}z}$ represents the normalized contribution of the ray scattered at each atmospheric layer to the total flux at surface. From radiative transfer calculations it can be shown that the effective scattering height ranges between 6.5 and 7.5 km above the station for a solar zenith angle (SZA) below 70°, which we estimate as the validity limit of the method.

Since both NO_2 and O_4 are analyzed in the same spectral range, the difference between the weighted center of the range for NO_2, i.e., the effective wavelength, and that of O_4, is small. The value of f is 0.9 for a near-Rayleigh atmosphere.

By using Eq. (2), the error introduced in NO_2 vmr due to the geometrical approximation, if assuming a constant mixing ratio of both O_4 and NO_2 with height, is 9.0 % at 70° SZA and 2.3 % at 50°. Since the scattering heights and the AMF are well known, the data can be corrected. The only uncertainty is due to the R value related to the vertical distribution of NO_2 within the FT. However, aircraft measurements over the ocean far from large industrial areas show that the tropospheric vertical distribution is nearly constant above the MBL (Bucsela et al., 2008).

In the presence of moderate or high aerosol loading at the level of the observational point, multiple scattering takes place and the method is no longer valid. Assuming that the aerosol layer is a well-mixed layer, we estimate an AOD of 0.1 at 500 nm as a safe limit (Gomez et al., 2014).

Since the path length is obtained from O_4 measurements, uncertainty in the magnitude of its absolute cross section is an additional source of error. It has been reported that paths obtained from O_4 are even larger than that RT computed for a Rayleigh atmosphere (Wagner et al., 2002) when using the generally accepted cross sections reported in the literature

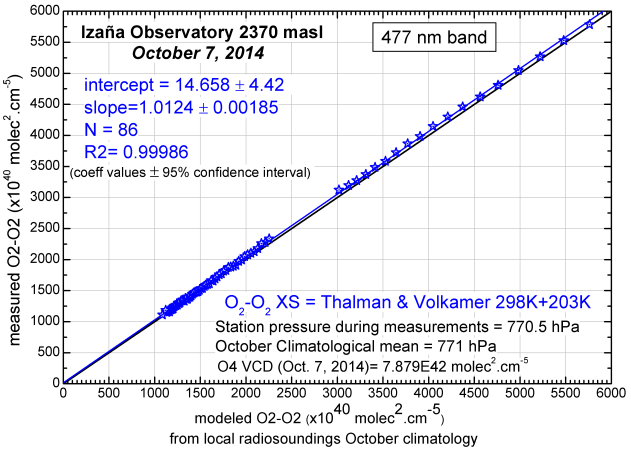

Figure 1. Measured O_4 slant column density versus modeled O_4 for a pure Rayleigh atmosphere at the 477 nm band by using cross sections at 203 and 293 K temperatures (see text for details).

(Greenblatt, 1990; Hermans, 2011), suggesting that cross sections are underestimated. There is, however, no agreement in the magnitude of the correct values. We performed direct Sun measurements on a very clear morning (aerosol optical density at 500 nm over the observatory was 0.007 ± 0.00077) at an O_4 effective temperature of 250 K, and compared the retrieved slant columns with the ones calculated from the local radio sounding of the day (7 October 2014) up to 30 km and the tropical standard atmosphere from 30 km upwards. Results show an excellent agreement with no difference at the error level when the retrieval includes O_4 cross sections at two temperatures (Fig. 1). In this exercise, the Thalman and Volkamer (2013) cross sections at 203 and 293 K were used. When including only the room temperature cross section in the retrieval, the obtained O_4 is 3–5 % too large.

Our results agree with the very recent report by Spinei et al. (2015) who found a temperature dependence of 9 % for a variation of 44 K and no pressure dependence based on direct Sun and aircraft MAXDOAS measurements. The conclusion of their work is that no corrections need to be made for effective temperatures near 275 K. Since the present method uses only the horizontal path, the temperature along the path is nearly constant and the seasonal variability in the subtropical FT is small. Air temperature at the level of Izaña ranges from 277 K in January–February to 287 K in July–August. Consequently, no more than 2 % of error is expected due to this effect.

Typical NO_2 slant column density (SCD) root-mean-square error of the fit for horizontal geometry is of 3×10^{14} molec. cm^{-2}. These errors represent 15–20 % of the typical differential SCD. A summary of the analysis errors is shown in Table 1.

Table 1. Method uncertainty.

Uncertainty in NO_2 due to fit	15–20 %
Uncertainty in path due to the O_4 fit	< 1 %
Uncertainty of the method (related to unknown vertical distribution of NO_2 and actual effective path)	2.5–9 % (for sza: 50 to 70°)
Error in horizontal path due to O_4 cross sections' temperature dependence	2 %
OVERALL UNCERTAINTY	20–32 %

3 The Izaña observatory and data set

Izaña (28.3° N, 16.5° W) is a well-known GAW-NDACC station located at the top of the Izaña Mountain, one of the peaks of the great crater of the Teide volcano, at 2370 m a.s.l., on Tenerife Island. The observatory and related meteorology has been extensively described in previous publications (i.e., Rodríguez et al., 2009; Cuevas et al., 2013). It is representative of the FT at night. During daytime it is frequently affected by anabatic winds resulting from heating of the ground. This upslope breeze carries boundary layer air masses to the FT. The intensity of the wind peaks near local noon and can extend well into the afternoon. It can be indirectly quantified using the measurements of water vapor on the station since air masses from below carry high humidity to the height of the observatory. The measurements of in situ NO_2 are also useful for this purpose, since the boundary layer (BL) NO_2 concentrations in populated areas near the coast are typically more than 1 order of magnitude larger than the background FT.

For the present work, only the horizontal spectra are analyzed. If the SZA was lower than 10°, then the 70° elevation spectrum was used as reference to avoid spectral distortions due to integration times that are too short. In all other cases, the reference was the zenith spectrum of the same cycle.

Data from 3 complete years (2011–2013) have been used after screening for (a) NO_2 RMSE: fit error is limited to 2×10^{15} molec. cm^{-2} and a signal to noise ratio of 0.5, which is approximately the detection limit of the instrument. (b) High SZA: only data corresponding to data below SZA 70° are used in the present analysis to limit the error in the path calculations. (c) Aerosol loading: measurements on days with aerosol optical depth (AOD) at 500 nm over 0.1 were rejected. (d) Length of the path: individual measurements with paths shorter than 30 km were also rejected (broken clouds or narrow dust layers might cause this effect). (e) Unrealistic negative values appeared occasionally. Over 15 000 data passed all filters for the 3-year period (40 % of all possible data).

4 The Optimal Estimation Method

The Optical Estimation Method (OEM) has been extensively used in the last years to obtain NO_2 vertical profiles of moderate to high polluted environments. However, on free troposphere background conditions, the concentrations are near the instrumental detection limit (10–100 pptv), and in these conditions, the method provides unrealistic profiles. In this work we have used it only to characterize the vertical distribution of the plume in a particular case study in which a high NO_2 air mass arrived at the station. The mean AOD at 500 nm on the studied day was only 0.02. Under these conditions the impact of the aerosol loading in the retrieval is very low. A test with and without aerosols yielded a mean difference of 1.6 % in the retrieval for heights between 1 and 5 km. Since uncertainties in the OEM method are larger than that value, aerosols have not been included in the analysis.

Given a set of measurements $\boldsymbol{y}$ with error covariance $\mathbf{S}_\varepsilon$, the OEM (Rodgers, 2000) provides the state vector $\boldsymbol{x}$ that maximizes the probability that $\boldsymbol{x}$, containing the trace gas vertical distribution, belongs to the interval $[\boldsymbol{x}, \boldsymbol{x} + \mathrm{d}\boldsymbol{x}]$. Following the OEM approach, the maximum a posteriori solution is calculated as

$$\begin{aligned}\hat{\boldsymbol{x}} &= \boldsymbol{x}_\mathrm{a} + \mathbf{S}_\mathrm{a}\mathbf{K}^T(\mathbf{K}\mathbf{S}_\mathrm{a}\mathbf{K}^T + \mathbf{S}_\epsilon)^{-1}(\boldsymbol{y} - \mathbf{K}\boldsymbol{x}_\mathrm{a}) \\ &= \boldsymbol{x}_\mathrm{a} + \mathbf{G}_y(\boldsymbol{y} - \mathbf{K}\boldsymbol{x}_\mathrm{a}),\end{aligned} \tag{4}$$

where the weighting functions matrix $\mathbf{K}$ expresses the sensitivity of the measurements to variations in the trace gas profile (NO_2 in this case). In this work, $\mathbf{K}$ is obtained with the SPSDISORT pseudo-spherical radiative transfer solver of the libRadtran software package (Mayer and Kylling, 2005). The $\boldsymbol{x}_\mathrm{a}$ vector and $\mathbf{S}_\mathrm{a}$ matrix correspond to an a priori NO_2 profile and its corresponding error covariance matrix, respectively.

The gain matrix $\mathbf{G}_y$, given by the following expression, quantifies the sensitivity of the retrieval to the measurements:

$$\mathbf{G}_y = \mathbf{S}_\mathrm{a}\mathbf{K}^T(\mathbf{K}\mathbf{S}_\mathrm{a}\mathbf{K}^T + \mathbf{S}_\epsilon)^{-1}. \tag{5}$$

The averaging kernel matrix $\mathbf{A}$, is then obtained as follows:

$$\mathbf{A} = \mathbf{G}_y\mathbf{K}. \tag{6}$$

$\mathbf{A}$ expresses the sensitivity of the retrieval to the true state, and it has an important role in the characterization of the retrieval. The retrieval at a given altitude is an average of the total profile weighted by the corresponding row of $\mathbf{A}$, also known as the averaging kernel function $\mathbf{AK}$. In general, the $\mathbf{AK}$s are functions with a single peak in the appropriate level, where the measurement provides additional information to add to the a priori profile. The trace of $\mathbf{A}$ provides the number of independent pieces that can be extracted from the re-

trieval, usually known as degrees of freedom (DFS). Typical values of the DFS in our retrievals are around 1.8.

Another parameter determining the quality of the retrievals is the total error of the state vector elements. This parameter is the addition of three contributions: (1) the smoothing of the true profiles given by $\mathbf{S}_a$; (2) the systematic errors of the measurements, provided by $\mathbf{S}_\varepsilon$ and (3) systematic errors of the forward model, mainly provided by the uncertainties in the parameters characterizing the atmosphere. Average total error (considering the three mentioned contributions) for all the considered profiles and altitudes ranging from 1 to 5 km is 0.01 ppb. The choice of the values corresponding to these three sources of error ($\mathbf{S}_a$, $\mathbf{S}_\varepsilon$ and the atmosphere parameters) in our study will be described in the following paragraphs.

The NO_2 hourly profiles used as a priori profiles in our calculations were obtained using a photochemical box model (Denis et al., 2005) derived from the SLIMCAT 3-D chemical transport model (Chipperfield, 2006). Diagonal elements of $\mathbf{S}_a$ are usually chosen to be a percentage of $\boldsymbol{x}_a$. In this case, following the L-curve method described in Schofield et al. (2003), they have been set to 100 % of $\boldsymbol{x}_a$, and its non-diagonal elements are calculated as follows (Barret et al., 2002; Friess et al., 2006):

$$\mathbf{S}_{aij} = \sqrt{\mathbf{S}_{aii}\mathbf{S}_{ajj}}\exp(-\ln(2)((z_i - z_j)/y)^2), \quad (7)$$

where z_i and z_j are the altitudes of the altitude grid levels i and j respectively, and γ is a half of the correlation length. The functions represented in the last equation are Gaussian correlation functions which account for correlations between trace gas concentrations at different altitudes. After several tests on the retrieval, γ value has been chosen to be 300 m, corresponding to the value (between 0.1 and 1 km) that maximizes the DFS (trace of $\mathbf{A}$), for the overall retrieval as well as for the altitudes closer to the station (2.3–2.6 km).

In this work, $\boldsymbol{y}$ represents the differential slant column densities (DSCD) of NO_2 measured with the MAXDOAS spectrometer, and $\mathbf{S}_\varepsilon$ is set to a diagonal matrix of which diagonal elements correspond to the molecular errors of the measurements.

Concerning parameters that characterize the atmosphere in our calculations, vertical profiles of O_3, O_2, CO_2 and H_2O have been obtained from the standard atmosphere for tropical latitudes (Anderson, 1986). Radio-sounding data performed the same day of our calculations provided the pressure, temperature and air density vertical profiles used in our retrieval. We have considered layers of 100 m from 0 to 10 km, and with the same width of those corresponding to the standard atmosphere for tropical latitudes (Anderson, 1986) for altitudes over 10 km. In this work, AKs are near zero for altitudes lower than 0.5 km and higher than 5 km (see Fig. 2). The retrieved profiles have been obtained for altitudes up to 6 km.

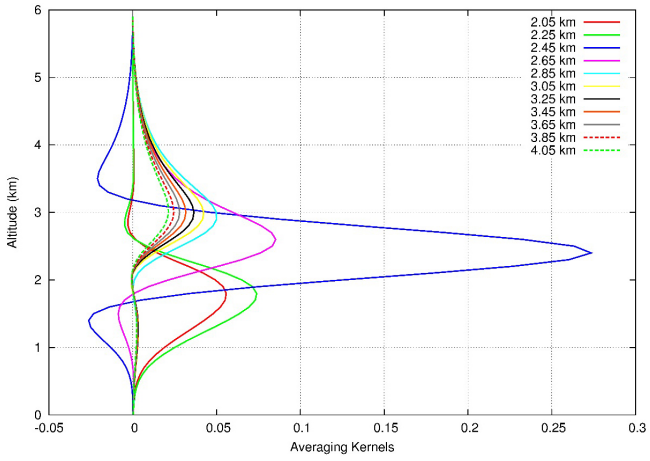

Figure 2. Example of NO_2 averaging kernels obtained in our profile retrieval, corresponding to 8 May 2013 at 12:00 UTC.

5 Model description and trajectory analysis

CAM-Chem (Community Atmosphere Model with chemistry) is a global 3-D chemistry–climate model fully integrated into the CESM (Community Earth System Model) framework (Lamarque et al., 2012). In this work, CAM-Chem has been configured using a horizontal grid resolution of 1.91 latitude × 2.5° longitude and 26 hybrid vertical levels from the surface to approximately 38 km. All simulations have been performed in specified dynamics (SD), using offline meteorological fields to compute the atmospheric transport, considering the same high-frequency meteorological input from a previous CAM-Chem 15-year simulation. This implies that the model is forced to evolve as if it were a chemical transport model.

The model includes the tropospheric chemistry mechanism of MOZART-4, implementing also organic and inorganic halogen (chlorine, bromine and iodine) photochemistry mechanisms, taking into account natural and anthropogenic sources, heterogeneous recycling and dry and wet deposition (Saiz-Lopez et al., 2012; Ordoñez et al., 2012; Fernandez et al., 2014). Anthropogenic emissions due to fossil fuel and biofuel combustions come from the POET (precursors of ozone and their effects in the troposphere) database for 2000.

To investigate the air masses reaching the area of study, back trajectories were computed with the HYSPLIT (Hybrid Single-Particle Lagrangian Integrated Trajectory) model, developed by NOAA Air Resources Laboratory (ARL) (Draxler et al., 2009). The ECMWF (European Centre for Medium-Range Weather Forecasts) meteorological fields were used with a spatial resolution of 0.25° × 0.25°, 22 vertical levels from the surface to 250 mb and a time resolution of 6 h. Three-dimensional kinematic back trajectories were calculated. A daily back trajectory at 12:00 UTC, with a 168 h pathway (7 days) at 2370 m a.s.l., was computed. Following the HYSPLIT model tools, back trajectories have been

grouped into clusters (Stunder, 1996), arriving at the Izaña observatory.

6 Results and discussion

6.1 MAXDOAS vs. in situ

Results of the NO_2 comparison can be classified according to three different meteorological regimes. A period in 2013 has been selected to illustrate the differences in concentration between the in situ local sampling and the MAXDOAS long-path average (Fig. 3, upper panel). On days when the breeze is inhibited, the in situ data are representative of the FT, and the agreement between instruments is very good (e.g., days 139–145). On days when anabatic winds are present, NO_2 vmr increases are observed in the in situ measurements, whereas the MAXDOAS signal remains at typical FT levels (e.g., days 130–137). Upslope winds cause an air mass mixture with that associated with the FT synoptic wind. The upslope strength will depend inversely on the intensity of the zonal synoptic winds (Cuevas et al., 2013). In general, the depth of the layer is not enough to contaminate the MAXDOAS path. This situation is the one most commonly observed at Izaña. As expected, MAXDOAS provides a much better representation of the FT background reactive gases. A third set of measurements is shown when MAXDOAS data also suffer large increases (e.g., days 127–129). After excluding thunderstorms with electric activity and wildfires in the area, it was found that this situation always takes place in the presence of southern winds. The only identified NO_2 large source upwind is the 980 MW thermal power plant located 25 km south of Izaña, with NO_2 emissions of 4.7×10^6 kg year^{-1}. As previously reported (Persson and Grazzini, 2007), the thermal local circulations are not captured by atmospheric global models, even by the ECMWF $0.25^\circ \times 0.25^\circ$ used in this study which predicted trajectories above 2000 m all the way (Fig. 3, lower right). This orographically forced lifting mechanism has been found to be an efficient and fast way for the irreversible transport of surface air to the FT. Pollutants and minor gases of oceanic origin (i.e., IO, BrO) move upslope, crossing the MBL top in less than 1 h, and then are subsequently mixed with FT air. The quantification of the amount of air mass transported from the lower layers of the MBL to the FT is outside of the scope of this work, but certainly data provide evidence for the existence of an efficient and fast mechanism to supply halogens and other marine trace gases to the FT. Since southern wind conditions are common during the summer months (50 % of the days) and the mountain rift has a NE–SW orientation, and a length of about 30 km, the supply of marine trace gases to the FT might not be negligible, at least on a local scale.

Surprisingly, the very high MAXDOAS vmr reaches as much as a half of the levels observed by the in situ sensor. This is related to the pointing direction of the DOAS spectrometer, since the plume propagates northward, along the same direction of the spectrometer line of sight. The path within the plume results in an enhancement of the absorption signal. Figure 4 shows the NO_2 vmr vertical cross sections for the day 128/2013, obtained by using the OEM technique, indicating that the enhancement takes place near the level of the station, with an upper limit around 4 km. This confirms that once the air mass passes over the mountain obstacle, it either moves horizontally or descends again but remains in the FT. Note that the instrument scanning lowest angle is below the horizon (IEA $= -1^\circ$), thus containing information about the trace gas concentration below the station.

It is worth mentioning that southern winds are generally related to African air masses containing Saharan dust and, as previously mentioned, those dusty days were filtered out from the analysis. The only non-dusty south wind cases observed are from Atlantic air masses which suffered an abrupt change in direction when approaching Africa. Consequently the impact of this effect on the overall data set is small. Only five clear cases have been identified within the 3-year record. Those cases have been removed for seasonal evolution studies.

Figure 5a shows the NO_2 vmr seasonal evolution separated by year. The seasonal behavior is similar in all 3 years, with the maximum in the summer months and the minimum in wintertime. Summer gaps result from the large number of Saharan dust intrusions during these months. To explore a possible dependence of the retrieved concentrations with the SZA, the data have been plotted in colors according the SZA (Fig. 5b). The maxima in summer months are observed, regardless of the SZA, excluding the possibility of stratospheric contamination or any other SZA-dependent artifact. The magnitudes of the retrieved concentration are also independent of the RMSE (Fig. 5c). Sporadic peaks over 100 pptv are observed with no increase in typical retrieval errors. The scattering through the day is also large with standard deviations of 10–15 pptv.

Monthly means clearly show the rapid spring build-up and the autumn decay (Fig. 6). Mean values range from 20 to 44 pptv throughout the year. A summer maximum has previously been found in unpolluted continental China in the boundary layer as a result of soil biogenic NO emissions (Van der A et al., 2006; Qi, 2015). However, NO_2 in long paths over the Atlantic FT cannot be explained in this way. The output of the CAM-Chem model for the location and the level of the station shows similar results. The agreement with observational data is particularly good for the period November to February. The NO_2 summer build-up takes place across the entire FT (not shown). The winter to summer ratio is largest in the middle troposphere at a height of 8 km. The peak FT NO_2 values occurring in summer were previously observed by Val-Martin et al. (2008), who attributed the summer maxima in NO_2 to North American biomass burning during this season. The model results show no seasonal differences in the NO_2 chemical formation/loss channels. However, an in-

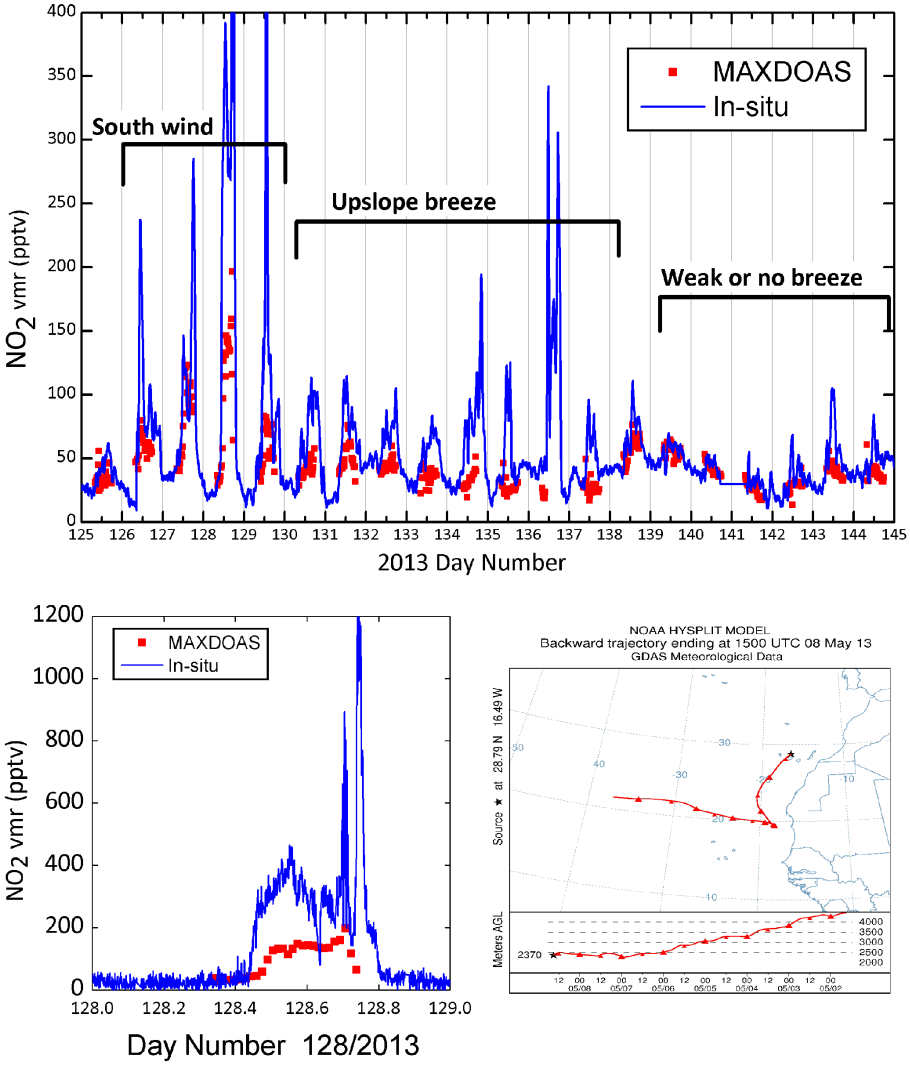

Figure 3. In situ NO_2 volume mixing ratio measurements made every minute versus Izaña MAXDOAS, for a period of time representative of three different wind situations. In situ data are smoothed by 50 min running mean (top panel). An expanded plot is shown for 8 May 2013 (day number 128). A back trajectory ending at Izaña at 15 h of the same day is shown.

crease in the overall reactive nitrogen budget occurs in this unpolluted FT site, as summer proceeds. We have explored two possibilities to explain the seasonality of our observations.

6.1.1 Contamination by anabatic winds

It has previously been shown that the MAXDOAS-MGA technique minimizes the unwanted effects of MBL on FT measurements, but in principle, the influence of a potential seasonal cycle in the intensity of the upwelling wind cannot be entirely ruled out. Since anabatic winds are driven locally by surface heating, the depth of the layer of influence is expected to be of only a few hundreds of meters, but there is not enough information to quantify the size of this depth and thus the potential contribution of a possible path contamination from air masses rich in NO_2 coming from below. Most of the works available in the literature refer to the BL, generally with return flowback. However, cases of upwelling to the FT are reported as well. As early as 1923, Wenger (1923) observed this situation at the slopes of the Teide mountain in Tenerife for up to 1500 m a.s.l., but no data were available above that height. In situ data in Fig. 1 show evidence of MBL nitrogen oxides transported by anabatic winds up to the level of the station (2370 m a.s.l.). However, an intensification of the upslope breeze in summer with respect to winter would result in a larger vertical extension of the upwelling layer, increasing its relative contribution in the MAXDOAS path. Out of the few large pollution cases, the concentrations measured are too low for the OEM technique to be applied. It is nevertheless unlikely that the summer increase in up-

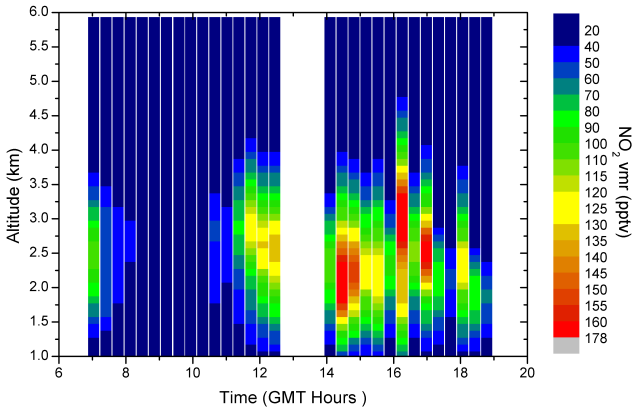

Figure 4. Unsmoothed vertical profiles of NO_2 vmr (in ppbv) for day 128/2013 obtained by the OEM technique. Each vertical column represents an individual scanning cycle (for details, see text).

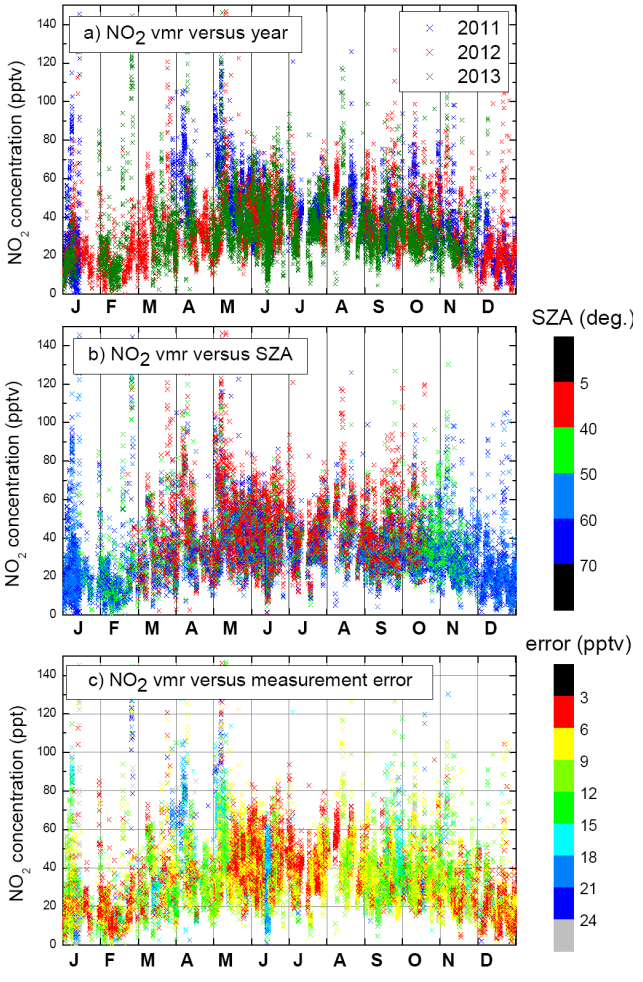

Figure 5. Seasonal evolution of the individual data NO_2 vmr separated by **(a)** years, **(b)** solar zenith angles and **(c)** RMSE.

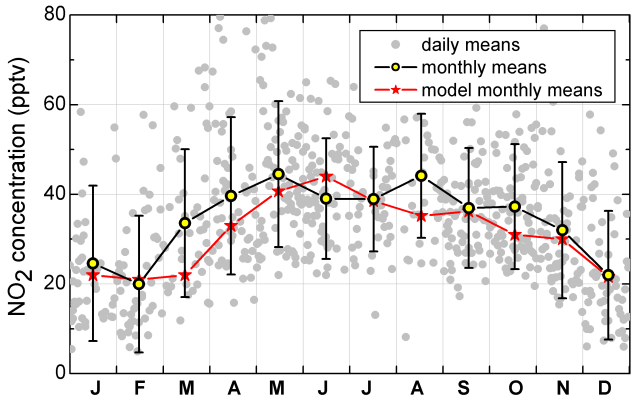

Figure 6. NO_2 concentration monthly means at the level of Izaña observatory with their respective standard deviations (open circles and black lines). CAM-Chem model results for the same level are shown for comparison (red stars and lines). Individual solid gray circles represent the 3-year diurnal mean.

welling can account for the twofold increase in the background NO_2 vmr. For instance, a layer of 200 m with a NO_2 load of as high as 600 ppt would represent an increase in the column of some 5–10 % of the background concentration for a clean day.

We have recalculated NO_2 monthly means only from the first morning data, namely data between SZA 70 and 65°. These SZA values correspond to fractional days ranging from 0.42 in midwinter to 0.32 in summer. At this early time of day, the anabatic wind is still under the first stage of development and the intensity of the upwelling is of only a few percent of the maximum value after noon. Results show that the seasonality in the SZA 65 to 70° data is almost identical to that when considering data at all SZA values (ratio > 0.98). We therefore conclude that the summer increase is not a result of the contamination by high NO_2 upwelled MBL air masses.

6.1.2 Changes in horizontal transport patterns through the season

Val-Martin et al. (2008) analyzed NO_2 mountain data from Azores and reported larger summer concentrations attributed to North American biomass burning. However, circulation at the lower latitudes of the Canary Islands is quite different. Attempts to determine the global FT distribution of NO_2, based on the cloud-slicing technique, have recently been made with OMI data (Choi et al., 2014), but the method does not provide results in summer over the Sahara region due to lack of cloudiness.

HYSPLIT 7-day back trajectory cluster analysis shows that air masses arriving at Izaña during the reported period are fundamentally of Atlantic origin, with a small portion arriving from Africa during the summer period (Fig. 7), in agreement with the 22-year (1988–2009) backward trajec-

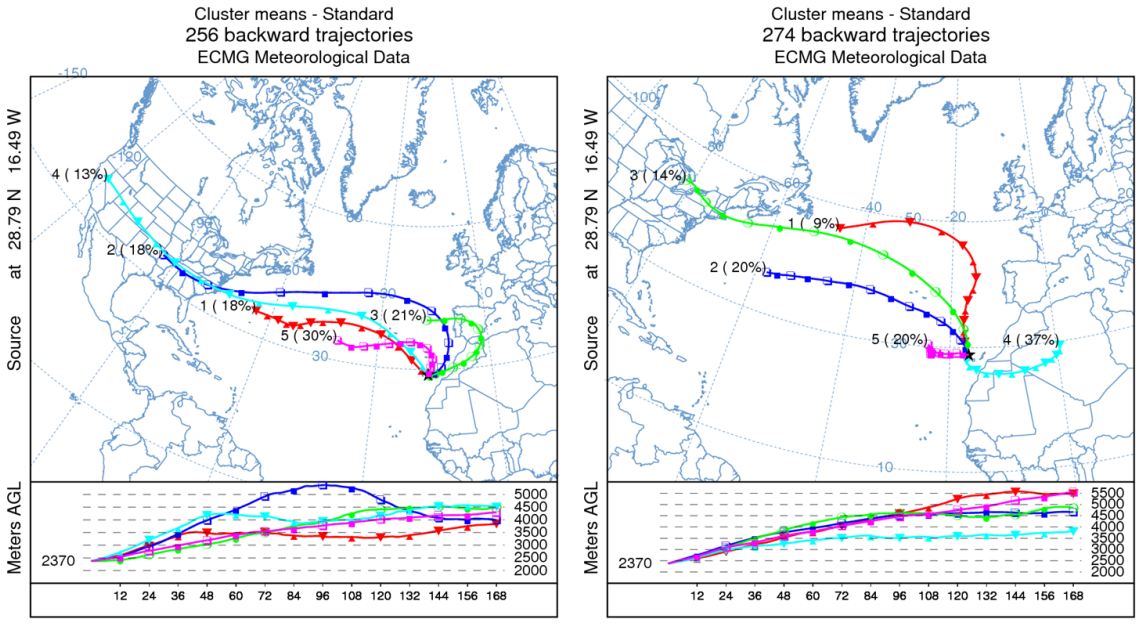

Figure 7. One-week HYSPLIT back trajectory clusters arriving at Izaña observatory for the winter months (DJF), left panel, and for the summer months (JJA), right panel, for the years 2011–2013.

tory climatology reported by Cuevas et al. (2013). As previously mentioned, only NO_2 observations under no-dust conditions are considered, therefore days with African trajectories are not included in the analysis. Winter trajectories are longer than the summer ones and 30 % of them cross the United States. All trajectory clusters show a steady descending transport in the last 96 h prior to the arrival at Izaña and originate at an altitude of 4000–5500 m a.s.l.

The cluster analysis tells us that the origin of the NO_2 seasonal variation has to be searched for in the western Atlantic area at much higher altitude than the Izaña station. The CAM-Chem model sampled at the 5.9 km level shows larger summer values over North America and the subtropical Atlantic than in winter months, both in the range of the observed values (Fig. 8). The phase of the mid-troposphere seasonal wave is opposite to the BL one (Lamsal et al., 2010) and is probably due to a combination of seasonality in convection and lightning. Venting processes from the BL to the FT over US have been studied (i.e., Parrish et al., 2004; Hudman et al., 2007), finding export of NO_y, mainly in the form of HNO_3 and PAN, to the mid-troposphere. Convection is driven by surface insolation and has a clear seasonal wave. The same is true for lightning, since thunderstorms mainly occur during the spring–summer months.

Tropospheric vertical profiles (Fig. 9) show how NO_2 vmr are decreasing in wintertime from the MBL to the mid-FT, whereas in summer the concentration remains constant up to 6 km and then increases. At the 5 km level, the model shows differences from 15 to 40 pptv from winter to summer. These calculated values are in agreement with the 40–50 pptv background NO_2 vmr estimated by Choi et al. (2014) for the summer months FT in an extended area covering the western Atlantic from subtropics to mid-latitudes.

The build-up is basically due to enhanced NO_2 formation via the $NO + O_3$ reaction under higher concentrations of NO as a result of NO_y reconversion of PAN and HNO_3 in the FT. Note that the lifetime of NO_y is long enough for NO_x-rich air masses, originated in North America, to reach the African coast.

In summary, the NO_2 seasonal variation obtained from MAXDOAS measurements can be explained with the help of the back trajectory cluster analysis and a chemistry–climate model and result from a mixed effect of long-range transport and free tropospheric subsidence. This is basically the same conceptual model that explains the origin or relatively high ozone values recorded at Izaña in summertime described by Cuevas et al. (2013). The origin of the high summer NO_2 values at Izaña is related to the larger background NO_2 vmr found over North America in the mid-FT, confirming earlier findings from Schultz et al. (1998).

7 Summary

NO_2 volume mixing ratio at the level of the high mountain observatory of Izaña (2370 m a.s.l.) has been obtained for 3 years of data using the MAXDOAS technique and the recently reported Modified Geometrical Approximation (MGA). The method uses the absorption of the O_2–O_2 collisional complex at 477 nm to obtain the horizontal path and is applicable in a near-Rayleigh atmosphere. Only data from air masses of aerosol optical depths below 0.1 were considered,

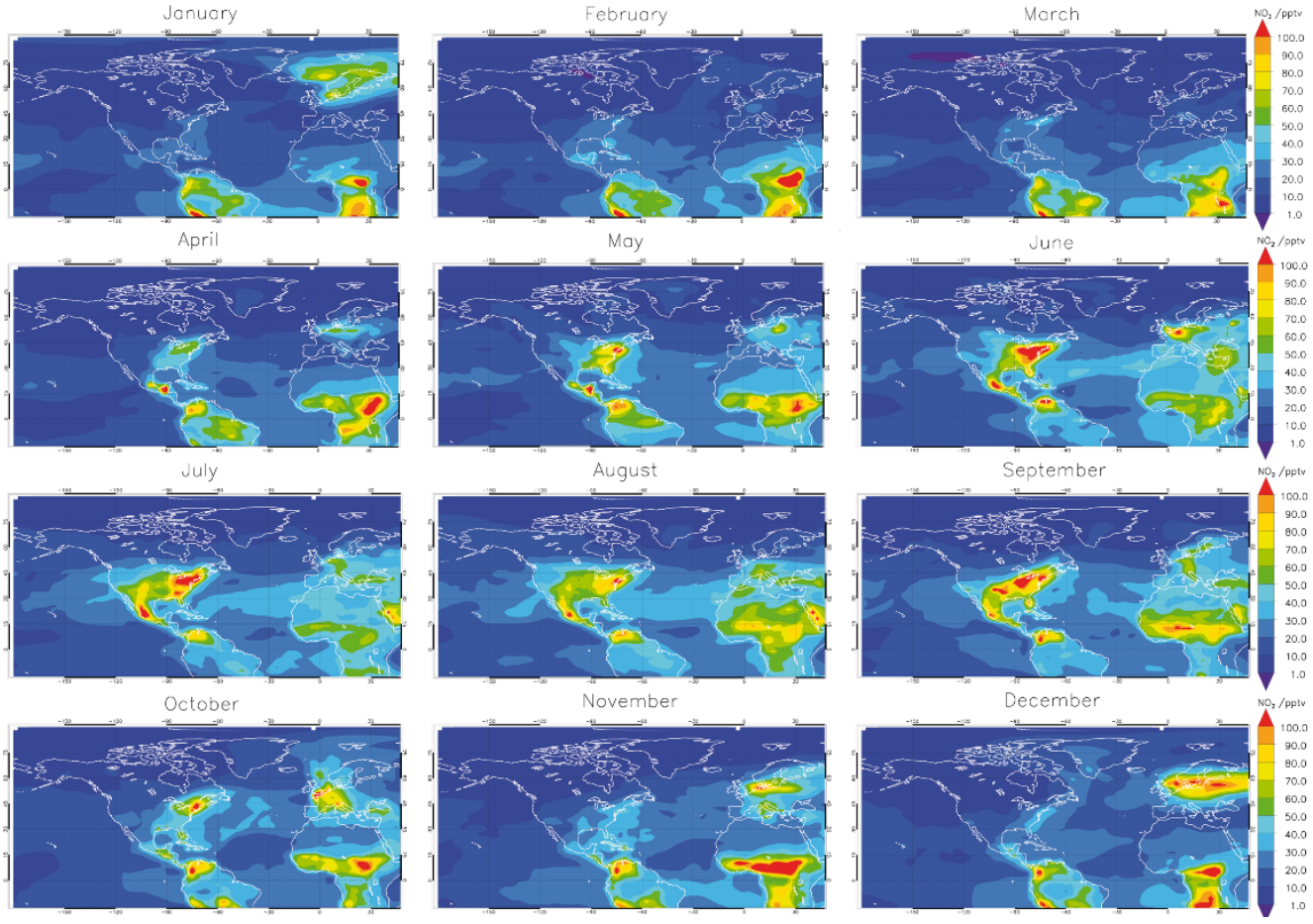

Figure 8. Global distributions of monthly mean NO_2 vmr for the level 5.9 km, obtained from the CAM-Chem chemistry–climate model.

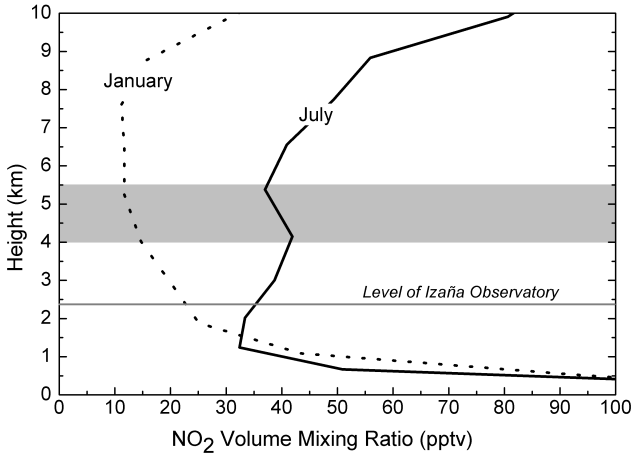

Figure 9. NO_2 vmr monthly mean vertical profiles from the CAM-Chem model. The gray band represents the height range where air masses are originated (see text).

thus removing African air masses loaded with Saharan dust. Results show that on most of the observation days, data are representative of the free troposphere. Exceptions are found when wind blows from the south. On these occasions, we find evidence that orographically forced surface air masses ascend upslope to the Izaña observatory, providing a channel for the irreversible transport of surface origin species to the free troposphere; this might provide an explanation for the concentrations of halogen oxides found in this region.

The NO_2 seasonal evolution shows a well-defined annual cycle in phase with solar radiation. Mean mixing ratios range from 20 pptv in midwinter to 42 pptv in summer with a significant day to day variability. By contrast, we find a small interannual variability during the 3-year observation period. A number of possible causes to explain the observed seasonality have been discussed, including seasonal changes in transport and contamination due to seasonality in the upslope winds (anabatic winds) but individually, they could not provide an explanation of the observations. The CAM-Chem chemistry–climate model reproduces the monthly distribution with great accuracy. The results of the back trajectory cluster together with the model analysis show that the season-

ality in NO_2 vmr is related to a combined effect of long-range transport and subsidence in the free troposphere. Dust-free trajectories follow North American/North Atlantic pathways, with air masses coming from the mid-free troposphere between 4000 and 5500 m a.s.l. The model and previous satellite estimations show a seasonality in NO_y and NO_2 in the mid-free troposphere in phase with the MAXDOAS observations at Izaña. Larger summer values are probably due to a combination of seasonality in convection and lightning.

Acknowledgements. This work was funded by the Spanish National R+D Funding Agency through the AMISOC (CGL2011-24891) project and the EU FP7 NORS project (grant agreement 284421). The authors gratefully acknowledge NOAA Air Resources Laboratory for the provision of the HYSPLIT transport and dispersion model.

Edited by: M. Van Roozendael

References

Anderson, G. P.: AFGL atmospheric constituent profiles (0–120 km), Hanscom AFB, MA: Optical Physics Division, Air Force Geophysics Laboratory, AFGL-TR; 86-0110, U.S. Air Force Geophysics Laboratory. Optical Physics Division, 1986.

Baidar, S., Oetjen, H., Coburn, S., Dix, B., Ortega, I., Sinreich, R., and Volkamer, R.: The CU Airborne MAX-DOAS instrument: vertical profiling of aerosol extinction and trace gases, Atmos. Meas. Tech., 6, 719–739, doi:10.5194/amt-6-719-2013, 2013.

Barret, B., De Maziere, M. D., and Demoulin, P.: Retrieval and characterization of ozone profiles from solar infrared spectra at the Jung-fraujoch, J. Geophys. Res., 107, 4788, doi:10.1029/2001JD001298, 2002.

Bradshaw, J., Newell, R., Sandholm, S., and Liu, S.: Observed distributions of nitrogen oxides in the remote free troposphere from the NASA Global Tropospheric Experiment Programs, R. Geophysics, 38, 61–116, 2000.

Bucsela, E. J., Perring, A. E., Cohen, R. C. Boersma, K. F., Celarier, E. A. Gleason, J. F., Wenig, M. O., Bertram, T. H., Wooldridge, P. J., Dirksen, R., and Veefkind, J. P.: Comparison of tropospheric NO_2 from in situ aircraft measurements with near-real-time and standard product data from OMI, J. Geophys. Res., 113, D16S31, doi:10.1029/2007JD008838, 2008.

Carroll, M. A., Hastie, D. R., Ridley, B. A., Rodgers, M. O., Torres, A. L., Davis, D. D., Bradshaw, J. D. Sandholm, S. T., Schiff, H. I., Karecki, D. R., Harris, G. W. Mackay, G. I., Gregory, G. L., Condin, E. P., Trainer, M., Hübler, G., Montzka, D. D., Madronic, S., H., Albritton, D. L., Singh, H. B., Beck, S. M., Shipham, M. C., and Bachmeier, A. S. Aircraft Measurements of NO_x over the Eastern Pacific and Continental United States and Implications for Ozone Production, J. Geophys. Res., 95, 10.205–10.233, 1990.

Chipperfield, M. P.: New version of the TOMCAT/SLIMCAT off-line chemical transport model: Intercomparison of stratospheric tracer experiments, Q. J. Roy. Meteorol. Soc., 132, 1179–1203, doi:10.1256/qj.05.51, 2006.

Choi, S., Joiner, J., Choi, Y., Duncan, B. N., Vasilkov, A., Krotkov, N., and Bucsela, E.: First estimates of global free-tropospheric NO_2 abundances derived using a cloud-slicing technique applied to satellite observations from the Aura Ozone Monitoring Instrument (OMI), Atmos. Chem. Phys., 14, 10565–10588, doi:10.5194/acp-14-10565-2014, 2014.

Cuevas, C., Notario, A., Adame, J. A., Hilboll, A., Richter, A., Burrows, J. P., and A. Saiz-Lopez: Evolution of NO_2 levels in Spain from 1996 to 2012, Scientific Reports, 4, 5887, doi:10.1038/srep05887, 2014.

Cuevas, E., González, Y., Rodríguez, S., Guerra, J. C., Gómez-Peláez, A. J., Alonso-Pérez, S., Bustos, J., and Milford, C.: Assessment of atmospheric processes driving ozone variations in the subtropical North Atlantic free troposphere, Atmos. Chem. Phys., 13, 1973–1998, doi:10.5194/acp-13-1973-2013, 2013.

Crutzen, P. J.: The Role of NO and NO_2 in the Chemistry of the Troposphere and Stratosphere, Annu. Rev. Earth Pl. Sc., 7, 443–472, doi:10.1146/annurev.ea.07.050179.002303, 1979.

Denis, L., Roscoe, H. K., Chipperfield, M. P., Van Roozendael, M., and Goutail, F.: A new software suite for NO_2 vertical profile retrieval from ground-based zenith-sky spectrometers, J. Quant. Spectrosc. Ra., 92, 321–333, doi:10.1016/j.jqsrt.2004.07.030, 2005.

Draxler, R. R., Stunder, B., Rolph, G., and Taylor, A.: HYSPLIT_4 User's Guide, via NOAA ARL website. NOAA Air Resources Laboratory, Silver Spring, MD, December 1997, revised January 2009, http://www.arl.noaa.gov/documents/reports/hysplit_user_guide.pdf (last access: 19 May 2015), 2009.

Fernandez, R. P., Salawitch, R. J., Kinnison, D. E., Lamarque, J.-F., and Saiz-Lopez, A.: Bromine partitioning in the tropical tropopause layer: implications for stratospheric injection, Atmos. Chem. Phys., 14, 13391–13410, doi:10.5194/acp-14-13391-2014, 2014.

Flynn, C. M., Pickering, K. E., Crawford, J. H., Lamsal, L. N., Krotkov, N. A., Herman, J., Weinheimer, A., Chen, G., Liu, X., Szykman, J., Tsay, S. C., Laughner, C. P., Hains, J., Lee, P., Dickerson, R. R., Stehr, J. W., and Brent, L.: The relationship between column.-density and 20 surface mixing ratio: statysdtical analysis, Atmos. Environ., 92, 429–441, 2014.

Friess, U., Monks, P. S., Remedios, J. J., Rozanov, A., Sinreich, R., Wagner, T., and Platt, U.: MAX-DOAS O_4 measurements: A new technique to derive information on atmospheric aerosols: 2. Modeling studies, J. Geophys. Res., 111, D14203, doi:10.1029/2005JD006618, 2006.

Gomez, L., Navarro-Comas, M., Puentedura, O., Gonzalez, Y., Cuevas, E., and Gil-Ojeda, M.: Long-path averaged mixing ratios of O_3 and NO_2 in the free troposphere from mountain MAX-DOAS, Atmos. Meas. Tech., 7, 3373–3386, doi:10.5194/amt-7-3373-2014, 2014.

Heland, J., Schlanger, H., Richter, A., and Burrows, J. P.: First comparison of tropospheric NO_2 column densities retrieved from GOME measurements and in situ aircraft profile measurements, Geophys. Res. Lett., 29, 1983, doi:10.1029/2002GL015528, 2002.

Hermans, C.: O_4 absorption cross-sections at 298 K (335.59–666.63 nm), available at: http://spectrolab.aeronomie.be/index.htm (last access: 19 May 2015), 2011.

Hilboll, A., Richter, A., and Burrows, J. P.: Long-term changes of tropospheric NO_2 over megacities derived from multiple

satellite instruments, Atmos. Chem. Phys., 13, 4145–4169, doi:10.5194/acp-13-4145-2013, 2013.

Hudman, R. C., Jacob, D. J., Turquety, S., Leibensperger, E. M., Murray, L. T., Wu, S., Gilliland, A. B., Avery, M., Bertram, T. H., Brune, W., Cohen, R. C., Dibb, J. E., Flocke, F. M., Fried, A., Holloway, J, Neuman, J. A., Orville, R., Perring, A., Ren, X., Sachse, G. W., Singh, H. B., Swanson, A., and Wooldridge, P. J.: Surface and lightning sources of nitrogen oxides over the United States: Magnitudes, chemical evolution, and outflow, J. Geophys. Res., 112, D12S05, doi:10.1029/2006JD007912, 2007.

Irie, H., Sudo, K., Akimoto, H., Richter, A. Burrows, J. P., Wagner, T., Wenig, M., Beirle, S., Kondo, Y., Sinyakov V. P., and Goutail, F.: Evaluation of long-rerm tropospheric NO_2 data obtained by GOME over East Asia in 1996–2002, Geophys. Res. Lett., 32, L11810, doi:10.1029/2005GL022770, 2005.

Isaksen, I. S. A., Zerefos, C., Kourtidis, K., Meleti, C., Dalsoren, S. B., Sundet, J. K., Grini, A., Zanis, P., and Balis, D.: Tropospheric ozone changes at unpolluted and semipolluted regions induced by stratospheric ozone changes, J. Geophys. Res., 110, D02302, doi:10.1029/2004JD004618, 2005.

Jacob, D. J., Crawford, J. H., Kleb, M.-M., Connors, V. S., Bendura, R. J., Raper, J. L., Sachse, G. W., Gille, J. G., Emmons, L., and Heald, C. L.: Transport and Chemical Evolution over the Pacific (TRACE-P) aircraft mission: Design, execution, and first results, J. Geophys. Res., 108, 9000, doi:10.1029/2002JD003276, 2003.

Kleissl, J. K., Honrath, R. E., Dziobak, M. P., Tanner, D., Val Martín, M., Owen, R. C., and Helmig, C,: The occurrence of upslope flows at the Pico mountain top observatory: A case study of orographic flows on a small, volcanic island, J. Geophys. Res., 112, D10S35, doi:10.1029/2006JD007565, 2007.

Lamarque, J.-F., Emmons, L. K., Hess, P. G., Kinnison, D. E., Tilmes, S., Vitt, F., Heald, C. L., Holland, E. A., Lauritzen, P. H., Neu, J., Orlando, J. J., Rasch, P. J., and Tyndall, G. K.: CAM-chem: description and evaluation of interactive atmospheric chemistry in the Community Earth System Model, Geosci. Model Dev., 5, 369–411, doi:10.5194/gmd-5-369-2012, 2012.

Lamsal R. N., Martin, R. V., van Donkelaar, A., Celarier, E. A., Bucsela, E. J., Boersma, K. F., Dirksen, R., Luo, C. and Wang, Y.: Indirect validation of tropospheric nitrogen dioxide retrieved from the OMI satellite instrument: Insight into the seasonal variation of nitrogen oxides at northern midlatitudes, J. Geophys. Res., 115, D05302, doi:10.1029/2009JD013351, 2010.

Liu, S. C., McFarland, M., Kley, D., Zafiriou, O., and Huebert, B.: Tropospheric NO_2 and O_3 budgets in the equatorial Pacific, J. Geophys. Res., 88, 1360–1368, 1983.

Mayer, B. and Kylling, A.: Technical note: The libRadtran software package for radiative transfer calculations – description and examples of use, Atmos. Chem. Phys., 5, 1855–1877, doi:10.5194/acp-5-1855-2005, 2005.

Ordóñez, C., Lamarque, J.-F., Tilmes, S., Kinnison, D. E., Atlas, E. L., Blake, D. R., Sousa Santos, G., Brasseur, G., and Saiz-Lopez, A.: Bromine and iodine chemistry in a global chemistry-climate model: description and evaluation of very short-lived oceanic sources, Atmos. Chem. Phys., 12, 1423–1447, doi:10.5194/acp-12-1423-2012, 2012.

Parrish, D. D., Ryerson, T. B., Holloway, J. S., Neuman, J. A., Roberts, J. M., Williams, J., Stroud, C. A., Frost, G. J., Trainer, M., Hübler, G., Fehsenfeld, F. C., Flocke, F., and Weinheimer, A. J.: Fraction and composition of NO_y transported in air masses lofted from the North American continental boundary layer, J. Geophys. Res., 109, doi:10.1029/2003JD004226, 2004.

Persson, A. and Grazzini, F., User Guide to ECMWF forecast products, Meteorological Bulletin M3.2, edited by: ECMWF, available at: http://www.uio.no/studier/emner/matnat/geofag/GEF4220/v09/undervisningsmateriale/Persson_user_guide.pdf (last access: 19 May 2015), updated 2007.

Puentedura, O., Gil, M., Saiz-Lopez, A., Hay, T., Navarro-Comas, M., Gómez-Pelaez, A., Cuevas, E., Iglesias, J., and Gomez, L.: Iodine monoxide in the north subtropical free troposphere, Atmos. Chem. Phys., 12, 4909–4921, doi:10.5194/acp-12-4909-2012, 2012.

Qi, Y.: Spatio-Temporal distributions of tropospheric NO_2 over Oases in Taklimakan Desert, China, Chin. Geogra. Sci., 25, 561–568, 2015.

Reidmiller, D. R., Jaffe, D. A., Fischer, E. V., and Finley, B.: Nitrogen oxides in the boundary layer and free troposphere at the Mt. Bachelor Observatory, Atmos. Chem. Phys., 10, 6043–6062, doi:10.5194/acp-10-6043-2010, 2010.

Richter, A., Burrows, J. P., Nüs, H., Granier C., and Niemeier, U.: Increase in tropospheric nitrogen dioxide over China observed from space, Nature, 437, 129–132, doi:10.1038/nature04092, 2005.

Ridley, B. A., Carroll, M. A., Gregory, G. L., and Sachse, G. W.: NO and NO_2 in the troposphere: Technique and measurements in regions of a folded tropopause, J. Geophys. Res., 93, 15813–15830, 1988.

Rodgers, C. D.: Inverse Methods for Atmospheric Sounding: Theory and Practice, vol. 2 of Atmospheric, Oceanic and Planetary Physics, World Scientific, Hackensack, NJ, doi:10.1142/9789812813718_fmatter, 2000.

Rodríguez, S., González, Y., Cuevas, E., Ramos, R., Romero, P. M., Abreu-Afonso, J., and Redondas, A.: Atmospheric nanoparticle observations in the low free troposphere during upward orographic flows at Izaña Mountain Observatory, Atmos. Chem. Phys., 9, 6319–6335, doi:10.5194/acp-9-6319-2009, 2009.

Saiz-Lopez, A., Lamarque, J.-F., Kinnison, D. E., Tilmes, S., Ordóñez, C., Orlando, J. J., Conley, A. J., Plane, J. M. C., Mahajan, A. S., Sousa Santos, G., Atlas, E. L., Blake, D. R., Sander, S. P., Schauffler, S., Thompson, A. M., and Brasseur, G.: Estimating the climate significance of halogen-driven ozone loss in the tropical marine troposphere, Atmos. Chem. Phys., 12, 3939–3949, doi:10.5194/acp-12-3939-2012, 2012.

Schultz, M., Schmitt, R., Thomas, K., and Volz-Thomas, A.: Photochemical box modeling of long-range transport from North America to Tenerife during the North Atlantic Regional Experiment (NARE) 1993, J. Geophys. Res. 103, 13477–13488, doi:10.1029/97JD01481, 1998.

Schofield, R.: The Vertical Distribution of Atmospheric BrO from Ground-Based Measurements, Ph.D. thesis, University of Auckland, available at: https://researchspace.auckland.ac.nz/handle/2292/357, (last access: 23 September 2015), 2003.

Spinei, E., Cede, A., Herman, J., Mount, G. H., Eloranta, E., Morley, B., Baidar, S., Dix, B., Ortega, I., Koenig, T., and Volkamer, R.: Ground-based direct-sun DOAS and airborne MAX-DOAS measurements of the collision-induced oxygen complex, O_2O_2, absorption with significant pressure and temperature differences,

Atmos. Meas. Tech., 8, 793–809, doi:10.5194/amt-8-793-2015, 2015.

Stunder, B.: An assessment of the Quality of Forecast Trajectories, J. Appl. Meteorol., 35, 1319–1331, 1996.

Thalman, R. and Volkamer, R.: Temperature dependent absorption cross-sections of O_2-O_2 collision pairs between 340 and 630 nm and at atmospherically relevant pressure, Phys. Chem. Chem. Phys., 15, 15371–15381, doi:10.1039/c3cp50968k, 2013.

Val-Martin, M., Honrath, R. E., Owen, R. C., and Li, Q. B.: Seasonal variation of nitrogen oxides in the central North Atlantic lower free troposphere, J. Geophys. Res., 113, D17307, doi:10.1029/2007JD009688, 2008.

Vandaele, A. C., Hermans, C., Simon, P. C., Carleer, M., Colins, R., Fally, S., Mérienne, M. F., Jenouvrier, A., and Coquart, B.: Measurements of the NO_2 Absorption Cross-Sections from 42000 cm^{-1} to 10000 cm^{-1} (238–1000 nm) at 220 K and 294 K, J. Quant. Spectrosc. Ra., 59, 171–184, doi:10.1016/S0022-4073(97)00168-4, 1998.

Wagner, T., von Friedeburg, C., Wening, M., Otten, C., and Platt, U.: UV-Visible observations of atmospheric O_4 absorptions using direct moonlight and zenith-scattered sunlight for clear sky and cloudy sky conditions, J. Geophys. Res., 107, 4424, doi:10.1029/2001JD001026, 2002.

Wenger, R.: Zur Theorie der Berg- und Talwinde', Meteorol. Z., 7, 193–204, 1923.

Wittrock, F., Oetjen, H., Richter, A., Fietkau, S., Medeke, T., Rozanov, A., and Burrows, J. P.: MAX-DOAS measurements of atmospheric trace gases in Ny-Ålesund – Radiative transfer studies and their application, Atmos. Chem. Phys., 4, 955–966, doi:10.5194/acp-4-955-2004, 2004.

Ziemke, J. R., Chandra, S., and Bhartia, P. K.: "Cloud slicing": a new technique to derive upper tropospheric ozone from satellite measurements, J. Geophys. Res., 106, 9853–9867, 2001.